

Research Paper

Comparison of ^{68}Ga -HBED-CC PSMA-PET/CT and multiparametric MRI for gross tumour volume detection in patients with primary prostate cancer based on slice by slice comparison with histopathology

Constantinos Zamboglou¹✉, Vanessa Drendel², Cordula A. Jilg³, Hans C. Rischke¹, Teresa I. Beck⁴, Wolfgang Schultze-Seemann³, Tobias Krauss⁵, Michael Mix⁴, Florian Schiller⁴, Ulrich Wetterauer³, Martin Werner², Mathias Langer⁵, Michael Bock⁵, Philipp T. Meyer⁴, Anca L. Grosu¹

1. Department of Radiation Oncology, Medical Center - University of Freiburg, Faculty of Medicine, University of Freiburg, Germany; German Cancer Consortium (DKTK), Partner Site Freiburg, Germany;
2. Department of Pathology, Medical Center - University of Freiburg, Faculty of Medicine, University of Freiburg, Germany; German Cancer Consortium (DKTK), Partner Site Freiburg, Germany;
3. Department of Urology, Medical Center - University of Freiburg, Faculty of Medicine, University of Freiburg, Germany; German Cancer Consortium (DKTK), Partner Site Freiburg, Germany;
4. Department of Nuclear Medicine, Medical Center - University of Freiburg, Faculty of Medicine, University of Freiburg, Germany; German Cancer Consortium (DKTK), Partner Site Freiburg, Germany;
5. Department of Radiology, Medical Center - University of Freiburg, Faculty of Medicine, University of Freiburg, Germany; German Cancer Consortium (DKTK), Partner Site Freiburg, Germany.

✉ Corresponding author: Constantinos Zamboglou, Department of Radiation Oncology, University Medical Center Freiburg, Germany, Robert-Koch Straße 3, D-79106 Freiburg. Telephone: +4976127094620 Telefax: +497612709582039670 Email: constantinos.zamboglou@uniklinik-freiburg.de.

© Ivyspring International Publisher. Reproduction is permitted for personal, noncommercial use, provided that the article is in whole, unmodified, and properly cited. See <http://ivyspring.com/terms> for terms and conditions.

Received: 2016.06.29; Accepted: 2016.09.11; Published: 2017.01.01

Abstract

Purpose: The exact detection and delineation of the intraprostatic tumour burden is crucial for treatment planning in primary prostate cancer (PCa). We compared ^{68}Ga -HBED-CC-PSMA PET/CT with multiparametric MRI (mpMRI) for diagnosis and tumour delineation in patients with primary PCa based on slice by slice correlation with histopathological reference material.

Methodology: Seven patients with histopathologically proven primary PCa underwent ^{68}Ga -HBED-CC-PSMA PET/CT and MRI followed by radical prostatectomy. Resected prostates were scanned by ex-vivo CT in a special localizer and prepared for histopathology. Invasive PCa was delineated on a HE stained histologic tissue slide and matched to ex-vivo CT to obtain gross tumor volume (GTV)-histo. Ex-vivo CT including GTV-histo and MRI data were matched to in-vivo CT(PET). Consensus contours based on MRI (GTV-MRI), PSMA PET (GTV-PET) or the combination of both (GTV-union/-intersection) were created. In each in-vivo CT slice the prostate was separated into 4 equal segments and sensitivity and specificity for PSMA PET and mpMRI were assessed by comparison with histological reference material. Furthermore, the spatial overlap between GTV-histo and GTV-PET/-MRI and the Sørensen-Dice coefficient (DSC) were calculated. In the case of multifocal PCa (4/7 patients), SUV values (PSMA PET) and ADC-values (diffusion weighted MRI) were obtained for each lesion.

Results: PSMA PET and mpMRI detected PCa in all patients. GTV-histo was detected in 225 of 340 segments (66.2%). Sensitivity and specificity for GTV-PET, GTV-MRI, GTV-union and GTV-intersection were 75% and 87%, 70% and 82%, 82% and 67%, 55% and 99%, respectively. GTV-histo had on average the highest overlap with GTV-union ($57\pm 22\%$), which was significantly higher than overlap with GTV-MRI ($p=0.016$) and GTV-PET ($p=0.016$), respectively. The mean DSC for GTV-union, GTV-PET and GTV-MRI was $0.51 (\pm 0.18)$, $0.45 (\pm 0.17)$ and $0.48 (\pm 0.19)$,

respectively. In every patient with multifocal PCa there was one lesion which had both the highest SUV and the lowest ADC-value (mean and max).

Conclusion: In a slice by slice analysis with histopathology, ^{68}Ga -HBED-CC-PSMA PET/CT and mpMRI showed high sensitivity and specificity in detection of primary PCa. A combination of both methods performed even better in terms of sensitivity (GTV-union) and specificity (GTV-intersection). A moderate to good spatial overlap with GTV-histo was observed for PSMA PET/CT and mpMRI alone which was significantly improved by GTV-union. Further studies are warranted to analyse the impact of these preliminary findings for diagnostic (multimodal guided TRUS biopsy) and therapeutic (focal therapy) strategies in primary PCa.

Key words: Prostate cancer, PSMA PET/CT, multiparametric MRI, histopathology.

Introduction

The accurate detection and delineation of intraprostatic tumour burden is important for diagnosis and treatment planning for patients with primary prostate cancer (PCa). Although PCa is mostly a multifocal disease, there is growing evidence that dominant intraprostatic lesions (DILs) may be responsible for metastatic and recurrent PCa [1, 2]. Focal therapy (e.g. radiotherapy, cryotherapy, laser therapy) targeting the DIL is of growing importance for the treatment of localized PCa [3].

Most of the ongoing studies use multiparametric magnetic resonance imaging (mpMRI) to define the gross tumour volume (GTV) for focal therapies [4]. However, our group [5] and others [6, 7] have validated the performance of radiolabelled tracers targeting the prostate-specific membrane antigen (PSMA) through comparison with histology, and have reported good results. PSMA is a transmembrane protein and it is expressed in PCa cells up to 1000 times higher than in normal prostate tissue [8]. For ligand binding to an extracellular domain of PSMA, specific inhibitors are used [9]. In this study we used a urea-based PSMA inhibitor conjugated with the chelator HBED-CC according to Eder et al. (^{68}Ga -Glu-NH-CO-NH-Lys(Ahx)-HBED-CC) [10]. Eiber et al. examined the value of ^{68}Ga -HBED-CC-PSMA PET/MRI hybrid imaging in 53 patients based on histological correlation on a sextant basis. The area under the receiver operating characteristics (ROC) curve was calculated for mpMRI (0.73), PSMA-PET/CT (0.83) and PSMA PET/MRI (0.88), respectively [11].

In this study seven patients underwent mpMRI and ^{68}Ga -HBED-CC-PSMA PET/CT before radical prostatectomy. We applied a procedure similar to that described by Grosu et al. [12] to match the histopathologic specimen after prostatectomy with ex-vivo CT. Subsequently, ex-vivo CT (including histopathology information, GTV-histo) and mpMRI data were matched to in-vivo CT, which was derived from PSMA PET/CT. GTV-PET, GTV-MRI and the

combination of both (GTV-union/-intersection) were created in analogy to the situation prior to targeted diagnostic or therapeutic interventions. The aim of this study is to evaluate the performance of ^{68}Ga -HBED-CC-PSMA PET/CT, mpMRI and the combination of both for detection and delineation of the tumour in patients with primary PCa based on histopathological reference on a slice by slice level.

Methods and Materials

Study design and patient population

We analysed data from a prospective, single institution study of 10 patients. Inclusion criteria were histopathologically proven primary adenocarcinoma of the prostate, pre-therapeutic ^{68}Ga -HBED-CC-PSMA PET/CT and intended radical prostatectomy. Exclusion criteria were neoadjuvant androgen deprivation therapy and previously performed transurethral resection of the prostate. MpMRI was not mandated in the original trial protocol, but was also performed in 7 patients. Mean patient age was 64 years (range 52-74) and mean serum PSA at imaging was 22.9 ng/ml (median 10.6, range 6.1-51.1, Table 1). Three patients had intermediate and four patients had high risk PCa, according to D'Amico's risk criteria [13]. Mean time between PET and MRI scan was 34 ± 30 days. Patients underwent radical prostatectomy on average within 18 ± 23 days after the last imaging examination. Written informed consent was obtained from each patient, and the institutional review board approved this study.

MR Imaging

MR images were acquired either on a 3 Tesla system (Trio Tim, Siemens, Germany / 4 patients) or on a 1.5 Tesla system (Aera and Avanto, Siemens, Germany / 3 patients). Both were equipped with surface phased array (Body Matrix) in combination with an integrated spine array coil. No endo-rectal RF coil was used. Following MR image data were included in this study:

T2-weighted turbo spin echo (TSE) images in the axial, sagittal and coronal planes with TR = 5500 ms (3 T)/ 8650-9400 ms (1.5 T); TE = 103-108 ms (3 T) / 111-119 ms (1.5 T); refocusing flip angle = 150°; field of view = 150 × 150 mm; slice thickness = 3 mm without gap; matrix: 192 × 192.

DWI with an echo planar imaging sequence in transverse orientation with TR = 3500 ms (3 T)/ 2800-3840 ms (1.5 T); TE = 73 ms (3 T) / 61-87 ms (1.5 T); flip angle = 90°; field of view = 250 × 250 mm (3 T) / (300 × 300) – (400 × 338) (1.5 T); slice thickness = 3 mm (3T) / 3–6 mm (1.5 T); slice gap: 0 mm (3 T) / 0-1,5 mm (1,5 T); matrix: 160 × 160 (3 T) / (192 × 162) – (160 × 160) (1.5 T), b values: 50, 400, 800 s/mm² (3 T) / 0; 100; 400; 800 or 0, 250, 500, 800 s/mm² (1.5 T).

DCE-MRI was acquired with dynamic 3D fast low-angle shot sequence in transverse orientation with TR = 5,13 ms (3 T)/ 4,65 – 4,1 ms (1,5 T); TE = 2,45 ms (3 T) / 1,58 - 1,6 ms (1,5); flip angle = 12° (3T) / 12° - 15° (1,5T); field of view = 260 × 260mm (3 T) / (260 × 260) – (400 × 387) (1,5 T); partition thickness = 3 mm (3T) / 2-3 mm (1.5 T); matrix: 192 × 192 (3 T) / (192 × 192) – (384 × 372) (1,5 T). Measurements were performed before, during and after an intravenous bolus injection of 0.2 ml/kg gadopentetate dimeglumine (Multihance, Bracco Imaging, Italy) at an infusion rate of 1 ml/s. 36 contrast-enhanced sets of 3D data were acquired sequentially at a temporal resolution of 9 s (3 T) / 7 s (1.5 T). No standardization algorithms for pre-processing [14] were used in the current study.

Table 1. Patient characteristics.

Patient	Age (y)	PSA (ng/ml)	TNM	Gleason score	mpMRI (Tesla)	PCa (% of prostate tissue)
1	67	6.07	pT3a pN1 cM0	3+4 (7a)	3	28
2	60	49	pT2c pN1 cM0	3+4 (7a)	1.5	56
3	59	9.15	pT2c pN0 cM0	4+3 (7b)	3	4
4	52	51.13	pT3b pN1 cM0	5+4 (9)	3	42
5	61	10.57	pT2c pN0 cM0	3+4 (7a)	3	15
6	74	8.82	pT2c pN0 cM0	3+4 (7a)	1.5	3
7	73	25.52	pT2c pN0 cM0	3+4 (7a)	1.5	4
Mean	64	22.89				22
SD ±	8	19.61				21.02

Abbreviations: PCa = prostate cancer. MpMRI = multiparametric MRI.

PET/CT Imaging

Radiolabelling of PSMA-HBED-CC with ⁶⁸GaCl₃ was done using a fully automated synthesis module (Eckert & Ziegler, Germany) in combination with

sterile single-use cassettes. The decay-corrected yield was >95% and the radiochemical purity of the final product was ≥97%.

The patients fasted for at least 4 hours before the administration of the radiopharmaceutical and were asked to void before starting the PET scan. 1 hour post injection, patients underwent the whole body PET scan. Scans were either performed with a 64-slice GEMINI TF PET/CT or a 16-slice GEMINI TF BIG BORE PET/CT (both Philips Healthcare, USA, pixel size 2x2x2 mm). Both scanners were cross-calibrated to ensure the comparability of the quantitative measurements. At the time of the PET scan, a contrast-enhanced diagnostic CT (120 kVp, 100-400 mAs, dose modulation, pixel size 1.172x1.172x2 mm) or a low-dose CT (120 kVp, 25 mAs, pixel size 1.172x1.172x2 mm) for attenuation correction (depending on previous CT scans and contraindications) was performed. The uptake of ⁶⁸Ga-PSMA-HBED-CC was quantified using standardized uptake values (SUV).

Histopathology/PET/CT/MRI image coregistration

Coregistration between PET/CT, MRI images and histopathology was performed in analogy to our published protocol [5, 12] (Figure 1). The resected prostates were fixed in a customized localizer (Medical Physics Laboratory) with a 4 mm grid and scanned using an ex-vivo CT (16-channel Phillips Brilliance Big Bore, Germany) was performed. Subsequently, the prostates were sectioned in a customized cutting device (Medical Physics Laboratory). Parallel 4-mm step-sections were cut perpendicular to the urethra at the same angle as the ex-vivo CT slices. PCa tissue was delineated on each histopathological slice using black ink. Histopathological slices were manually matched to the ex-vivo CT using MITK software (MITK Workbench 2014.10.00; German Cancer Research Center) with the guidance of the 4 mm grid and radiopaque markers within the prostate. The histopathological PCa contours were digitized from the step-sections to corresponding ex-vivo CT slices and automatically interpolated in MITK to create GTV-histo. A careful manual coregistration with additional non-rigid deformation between ex-vivo CT (including GTV-histo) and in-vivo CT (PET/CT scan) was performed in MITK. After registration, the overlap of the prostatic gland in ex-vivo and in-vivo CT was evaluated in 3 patients (low, intermediate and high tumor burden) by median distance (MD) and dice similarity (DSC). MD was calculated by:

$$MD = \text{median} \left(\bigwedge_{a \in A} d(a, B), \bigwedge_{b \in B} d(b, A) \right)$$

Where $\bigwedge_{a \in A} d(a, B)$ represented the distances of all points a in contour A to contour B . Additionally, the DSC was calculated by: $DSC = 2|A \cap B| / (|A| + |B|)$. MD was below the PET image resolution (range: 1.2 to 1.7 mm). The DSC ranged from 0.83 to 0.88, which translated into an excellent overlap. Visual assessment of the contours showed that no anatomically implausible deformations took place.

In-vivo PET/CT datasets (including GTV-histo) of each patient were imported into the radiation treatment planning system (iPLAN RT image 4.1; BrainLAB, Germany). Axial TSE-, DWI- (ADC maps) and DCE-MRI images were automatically matched with in-vivo CT images using mutual information registration in iPlan. If visual assessment showed anatomical mismatch, a manual adjustment was performed based on anatomical markers. For alignment between PET and CT scans the preset registration was used. Thus, CT/PET/MRI and histopathology data were registered in the same reference frame which is a prerequisite for evaluating them comparatively slice by slice.

Generation of contours

Image analysis was done in iPLAN. Two experienced radiologists (HCR and TK) delineated GTV-MRI in consensus using T2W, DWI and DCE-sequences to characterize each lesion. Areas with visually determined PI-RADS v2 [15] score ≥ 4

were included in the analysis. With respect to PI-RADS v2 criteria and score for delineation of peripheral zone lesions, DWI images were of top priority and in case of score 3 lesions, DCE images were used to obtain final PI-RADS category (e.g. if focal and early enhancement was present, the lesion or part of it was classified with score 4 and enclosed to the GTV). T2W-TSE images were primarily used for delineation of transition zone lesions. According to PI-RADS v2 TZ-lesions with score 3 at T2W were classified as score 4 if DWI suggested markedly hyperintense signal on high b-value DWI/markedly hypointense signal on ADC. These suspicious areas were enclosed to the GTV.

GTV-PET was delineated in consensus by two experienced nuclear medicine physicians (TIB and PTM) using window levels from 0-5 SUV. Any focal uptake distinctly higher than local background was considered to represent PCa. A union volume (GTV-union) and an intersection volume (GTV-intersection) between GTV-PET and GTV-MRI were created for each patient.

Slice by slice analysis

We calculated sensitivity and specificity for PSMA PET, mpMRI and the combined volumes (GTV-union/-intersection) based on histology reference data. The prostate in each in-vivo CT slice was divided into 4 equal segments (Figure 2) and the analysis was performed visually using the GTVs obtained. A mean of 48 segments (± 14) per patient were analysed.

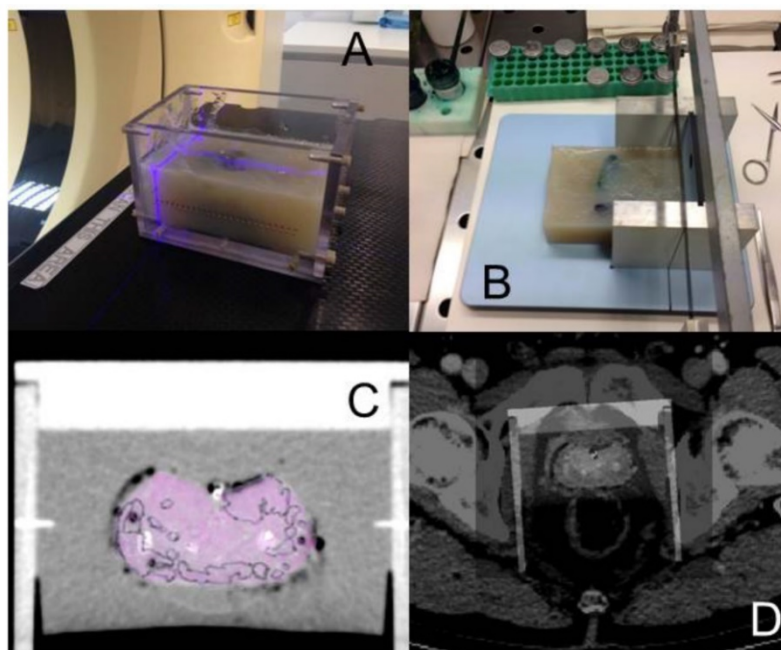


Figure 1 The resected prostate was embedded in agar in a localizer with a 4 mm marker profile and ex-vivo CT was performed by using reference points on the localizer for orientation (A). In a cutting device 4 mm step sections were cut (B). Whole-mount sections and ex-vivo CT images were merged under the guidance of markers on the localizer (C). Ex-vivo and in-vivo prostate were registered manually by two specialists in consensus (D).

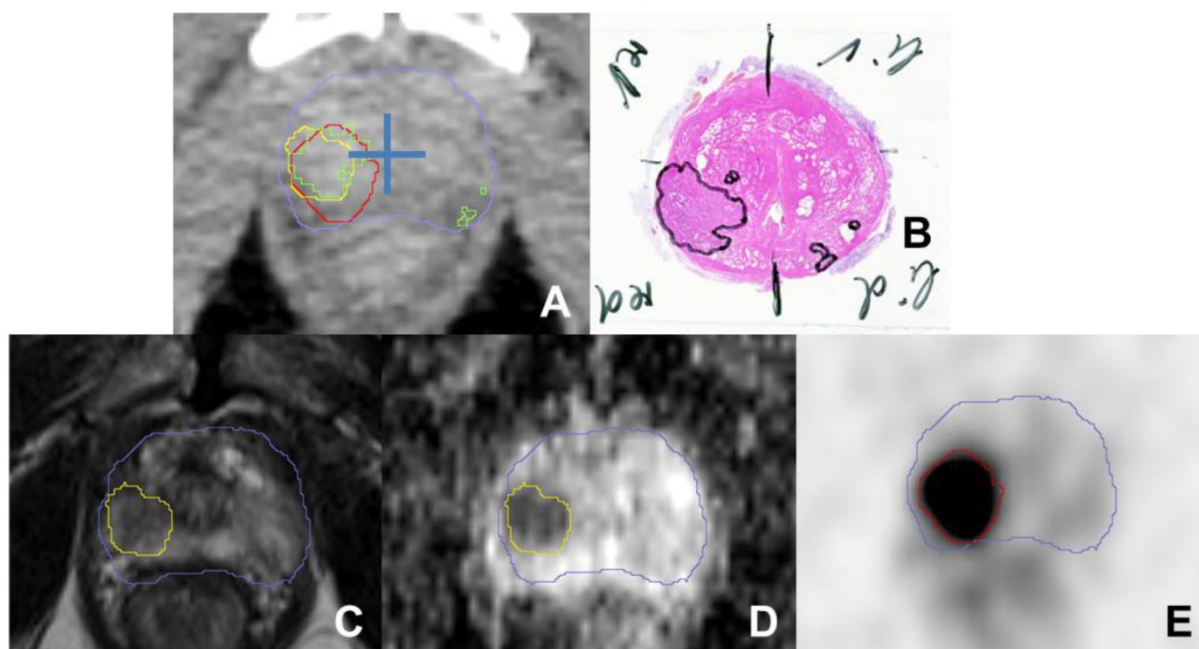


Figure 2 A shows a transverse CT image (from PSMA PET/CT scan) with projected GTVs (green: histology, red: consensus GTV PSMA PET, yellow: MRI) for patient 4. The blue cross was placed in the middle of the prostate to separate each CT slice into four quadrants to analyse sensitivity and specificity. Haematoxylin and eosin gross section histopathology shows a large tumour focus in the right lobe and small foci in the left peripheral zone (B). Transverse T2-weighted image (C) shows a slightly hypointense signal with restricted diffusion in the apparent ADC map (D). PSMA PET image (E) shows intense focal uptake located in the right lobe. The blue contour represents the prostatic border in the corresponding CT scan.

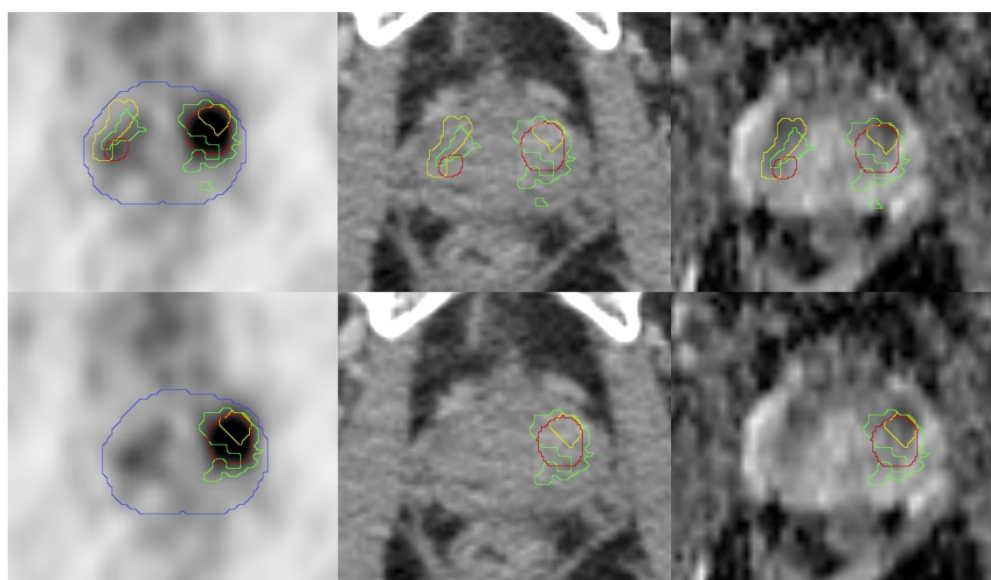


Figure 3 Pictures from left to right show: transverse PET images, CT images (both from ^{68}Ga -HBED-CC-PSMA PET/CT scan), ADC-MR images from patient 5. PET and CT images are presented with projected GTVs (green: histology, red: SUV30, yellow: MRI). The blue contour represents the prostate border in the corresponding CT scan. In the upper row the entire histopathologically defined PCa was taken into account. In the lower row only the lesions with the highest SUVmean (PET) or ADC-value (ADC-MRI) were projected. The corresponding lesion in histology was defined as GTV-histo.

Analysis of spatial overlap

We calculated the percentage of GTV-histo which overlapped with the imaging derived GTVs and the DSC was calculated.

Detection of dominant intraprostatic lesions

Some preclinical and clinical studies indicated

that low ADC-values in DWI-MRI [16] and high SUV values in PSMA PET [6, 17, 18] may indicate potential DILs. In the case of multiple lesions in PET (4/7) and MRI (4/7) we defined the lesion with the highest SUV value (mean and max) as GTV^{DIL}-PET and the lesion with the lowest ADC-value (mean and max) as GTV^{DIL}-MRI. Subsequently, the corresponding lesion in histology was defined as GTV^{DIL}-histo (Figure 3).

Statistical analysis

Statistical analysis was performed with MATLAB (MATLAB R2014a, The MathWorks, USA) and Microsoft Excel 2010 (Microsoft, Redmond, USA). The Wilcoxon signed-rank test, Wilcoxon rank-sum test and Spearman's Rho test were used with a threshold for statistical significance of <0.05.

Results

I Sensitivity and specificity

PCa was detected by ^{68}Ga -HBED-CC-PSMA PET/CT and by mpMRI in all patients. GTV-histo was observed in 225 of 340 segments (66.2%). Sensitivity and specificity for GTV-PET and GTV-MRI were 75% and 87%, 70% and 82%, respectively (Table 2). GTV-PET identified 24 PCa-involved segments classed as negative by mpMRI, whereas 21 true positive segments were observed by GTV-MRI classed as negative by PET. GTV-union had the highest sensitivity (82%) and the lowest specificity (67%), whereas GTV-intersection had the highest specificity (99%) and the lowest sensitivity (55%). PCa localization, post prostatectomy Gleason score, amount of prostatic tumour tissue, and serum PSA level before imaging had no correlation with sensitivity of PSMA PET/CT and MR imaging (Table 3).

Table 2. Correlation metrics.

Parameter	% of GTV-histo in overlap	DSC	Sensitivity (%)	Specificity (%)
GTV-MRI	42 (± 18)	0.48 (± 0.19)	70 (± 22)	82 (± 19)
GTV-PET	45 (± 24)	0.45 (± 0.18)	75 (± 11)	87 (± 16)
GTV-union	57 (± 22)	0.51 (± 0.18)	82 (± 14)	67 (± 36)
GTV-intersection	22 (± 17)	0.38 (± 0.21)	55 (± 25)	99 (± 2)

Abbreviations: DSC = Sørensen-Dice coefficient. GTV = gross tumor volume, which was based on MRI, PSMA PET or the combination (union or intersection) of both.

Table 3. Influence of clinical parameters on Sensitivity of PSMA PET and mpMRI.

Patient	Sensitivity MRI	Sensitivity PET	Localization of GTV-histo	Gleason score	PCa (% of prostate tissue)	PSA (ng/ml)
1	0.61	0.87	a, m, b	7a (3+4)	28	6.07
2	0.68	0.83	a, m, b	7a (3+4)	56	49
3	0.33	0.78	a	7b (4+3)	4	9.15
4	0.94	0.80	a, m, b	9 (5+4)	42	51.13
5	0.69	0.54	a, m	7a (3+4)	15	10.57
6	0.63	0.63	m, b	7a (3+4)	3	8.82
7	1	0.8	a	7a (3+4)	4	25.52

The influence of localization of GTV-histo, post prostatectomy Gleason score, amount of prostatic tumour tissue and serum PSA level before imaging on sensitivity of PSMA PET/CT and MRI was evaluated. No correlation was found for Gleason score, amount of prostatic tumour tissue and serum PSA level using Spearman's Rho test ($p > 0.05$ for all parameters). No correlation was found for PCa localization using Wilcoxon rank-sum test ($p > 0.05$). Abbreviations: the localization of PCa was classified as a = apical, m = mid-gland, b = base.

II Spatial overlap with GTV-histo

Mean volumes were 7.1 ± 8.6 ml (GTV-PET), 5.3 ± 5.9 ml (GTV-MRI), 9.1 ± 9.8 ml (GTV-union) and 3 ± 3.9 ml (GTV-intersection), respectively, and mean GTV-histo was 7.3 ± 7.5 ml. GTV-histo had the highest mean overlap with GTV-union, $57 \pm 22\%$ (Table 2, Figure 4), which was significantly higher than overlap with GTV-MRI ($p=0.016$) and GTV-PET ($p=0.016$), respectively. The mean DSC for GTV-union, GTV-intersection, GTV-PET and GTV-MRI was 0.51 ± 0.18 , 0.38 ± 0.21 , 0.45 ± 0.17 and 0.48 ± 0.19 , respectively.

III Detection of the DIL

^{68}Ga -HBED-CC-PSMA PET/CT and mpMRI depicted the same lesion (Figure 3) as the DIL in all patients (4 out of 7) with multifocal PCa. Each lesion with the highest SUVmean or SUVmax corresponded to the lesion with the lowest mean or maximum ADC-value. For all DILs the average SUVmean and SUVmax were 4.47 ± 0.75 and 8.16 ± 3.36 , respectively, whereas the mean ADC-value and the maximum ADC-value were 0.880 ± 0.08 mm^2/sec and 1.680 ± 0.16 mm^2/sec , respectively. Mean $\text{GTV}^{\text{DIL}}\text{-PET}$ and $\text{GTV}^{\text{DIL}}\text{-MRI}$ was 2.5 ± 1.7 ml and 1.3 ± 1.2 ml, respectively. Mean $\text{GTV}^{\text{DIL}}\text{-histo}$ was 2.7 ± 2 ml, whereas mean GTV-histo was 3.51 ± 2.4 ml in these patients.

Discussion

Numerous studies postulated a good performance for mpMRI in detection and delineation of primary PCa [19] and current guidelines propose mpMRI for local staging in primary PCa [20]. Our group compared histology (biopsy), ^{68}Ga -HBED-CC-PSMA PET/CT and mpMRI for GTV delineation in patients with primary PCa and reported discrepant results in half of the patients [21]. Based on a method described by Grosu et al. [12], we compared ^{68}Ga -HBED-CC-PSMA PET/CT and histology after prostatectomy on a voxel level and demonstrated a high spatial overlap with a mean area under the ROC curve of 0.83 [5].

This is the first study performing a slice by slice comparison between ^{68}Ga -HBED-CC-PSMA PET/CT, mpMRI and whole-mount histopathology. We could confirm the good performance of mpMRI and PSMA PET/CT, respectively, for localization and delineation of primary PCa, which was further enhanced by multimodal imaging using combined PSMA PET and mpMRI information. These findings may be implemented in treatment (focal therapy) and diagnostic (PET/MRI-guided biopsy) strategies for primary PCa.

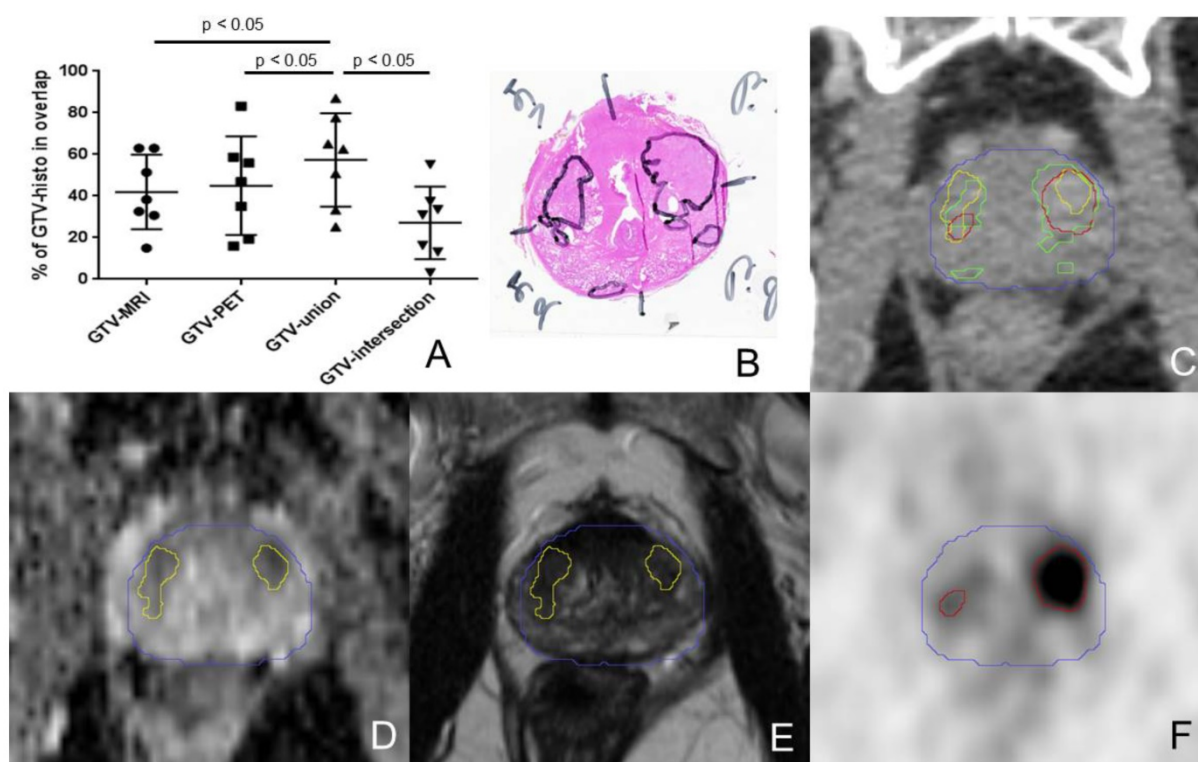


Figure 4 The percentage overlaps between GTV-histo and the GTVs defined by imaging are shown in A. The middle bars represent the mean values and the upper and lower bars the standard deviations. The overlap with GTV-histo was significant higher for GTV-union compared to GTV-MRI, GTV-PET and GTV-intersection ($p < 0.05$) in Wilcoxon signed-rank test. B shows haematoxylin and eosin gross section histopathology with two large tumour foci in each side of the prostate of patient 7. An axial CT image (from PSMA PET/CT scan) with projected GTVs (green: histology, red: PET, yellow: MRI, blue: contour of prostate gland in in-vivo CT) is presented in C. In the lower row ADC-MRI (D) and T2w-MRI (E) are presented with corresponding GTV-MRI. F shows GTV-PET projected on the corresponding axial PSMA PET slice. In the left lobe GTV-PET overlaps better with GTV histo than does GTV-MRI. In the right lobe GTV-MRI has a higher coverage of GTV-histo.

In detail, the addition of GTV-PET and GTV-MRI to GTV-union increased sensitivity (82%) compared with PSMA PET (75%) or mpMRI (70%) alone. Two studies reported lower sensitivities for PSMA PET (64% and 49%), mpMRI (58% and 44%) and PSMA PET/MRI (76%, only [11]), although the relationship between the observed sensitivities is similar [11, 22]. In total, 225 segments involved PCa. Of these 24 (10.7%) and 21 (9.3%) were identified by PSMA PET/CT or mpMRI, respectively, while classed as negative by the other imaging modality. This finding is consistent with Eiber et al. [11] who stated that each method is able to identify PCa-involved areas classed as negative by the other modality. A meta-analysis of recent studies calculated a pooled sensitivity for mpMRI of 78% (64.9–95%) [19]. The specificity was slightly higher for PSMA PET than for mpMRI or GTV-union (87%, 82%, 67% respectively). This finding is similar to three recent studies [6, 11, 22], which reported higher specificities for PSMA PET (94–96%) than for mpMRI (82–94%). The range for sensitivity and specificity is likely due to a lack of standardization in data acquisition and in data analysis.

Combined ^{68}Ga -HBED-CC-PSMA PET/CT and MR imaging led to increased overlap with GTV-histo

(GTV-union 57%, GTV-PET 45%, and GTV-MRI 42%), which was statistically significant. The average GTV increased when it was delineated by PET (7.1 ml) compared to mpMRI (5.3 ml). This finding is consistent with previous studies [21, 23]. Physical properties of PET (e.g. spill-over effect) may serve as a possible explanation. The addition of PET and mpMRI (GTV-union) led to an average volume of 9.1 ml, which was larger than mean GTV-histo (7.3 ml). Likewise, the average DSC was similar for GTV-PET (0.45), GTV-MRI (0.48) and GTV-union (0.51). Chang et al. reported similar DSC values of 0.52 and 0.37 for manually delineated ^{11}C -choline PET/CT and MRI contours, respectively [24]. Focal therapy approaches targeting GTV-union may possess an overtreatment of healthy tissue (lower specificity and larger volumes). Thus, we also analysed intersection volumes (GTV-intersection) between PET and mpMRI, which showed a low average overlap with 27% of GTV-histo and a low sensitivity (55%) but a high specificity of 99%. It should be mentioned that mean GTV-intersection (3 ml) was significantly smaller than mean GTV-histo (7.3 ml). A previous study compared ^{68}Ga -HBED-CC-PSMA PET/CT and mpMRI for GTV delineation within the prostate in 22 patients with primary PCa. On average, 40% of the

PET based volume was in intersection with MRI based GTVs [21]. Thus, the existence of complementary information between PSMA PET/CT and mpMRI could serve as a possible explanation for the small intersection volumes. A mismatch in coregistration between MRI and PET/CT images may have also led to small GTV-intersection. In the future, studies should evaluate whether these intersection regions may host higher Gleason scores, increased tumour stem cells [25], or hypoxic regions, which may be predictors for biochemical failure after radiation therapy [26]. The intersection volumes may contain a high probability of significant PCa and may be treated more intensely in order to improve tumour control. Additionally to the solely visual definition of GTV-PET, we applied an automatic threshold of 30% of SUVmax within the prostate to define GTV-PET^{30%}. This threshold was derived from a previous voxel-wise correlation between PSMA PET/CT and histology using receiver operating characteristic (ROC) requesting a sensitivity ≥ 0.9 [5]. The analyses were performed in the same patient population and were likewise not used for comparison with MR imaging. We observed an increased overlap with GTV-histo (58%) and an increase in sensitivity (83%) but a decrease in specificity (65%). The union volume between GTV-MRI and GTV-PET^{30%} had a sensitivity of 88% and overlapped with 70% of GTV-histo.

Our data indicated a potential advantage of ⁶⁸Ga-HBED-CC-PSMA PET/CT over mpMRI in terms of mean overlap with GTV-histo, specificity and sensitivity. It should be mentioned that ex-vivo CT (including GTV-histo) was matched to in-vivo CT derived from combined PSMA PET/CT scans. MR images were subsequently matched to in-vivo CT. Thus, a potential error in coregistration between MRI and in-vivo CT may mislead the correlation with histology. Chang et al. compared mpMRI with choline PET/CT for GTV-delineation in primary PCa based on histological reference data using a similar approach to our study, with the difference that histology was directly matched to MR images [24]. They reported a DSC of 0.37 for manually delineated MRI contours, which was lower than the DSC for GTV-MRI in our study (0.42). However, MRI had a higher sensitivity than GTV-PET in 3 out of 7 patients. Further studies are warranted to characterize patient populations (e.g. by tumor localization, Gleason score or PSA levels) in which the combined usage of PSMA PET and mpMRI is necessary or only one image modality is sufficient. In our study no clinical parameter had a significant correlation with sensitivity of mpMRI or PSMA PET/CT. This may be due to the limited number of cases and relatively small variability, since 5 of 7 patients had a Gleason

7a (3+4).

In addition to the global PCa distribution, we examined the value of ⁶⁸Ga-HBED-CC-PSMA PET/CT and mpMRI for detecting of the potential DIL. There are no conclusive data on which histopathological parameters should be used to define DIL. Stamey and co-workers have established the hypothesis that prognosis may be related mainly to the volume and histological grade of the largest cancer in the prostate [27, 28]. However, the lesion with the highest Gleason score may not always be the lesion that endangers the patient the most. As shown by Haffner et al. [29], even a Gleason 6 (3+3) lesion may be eventually lethal. Thus, we used parameters derived from multimodal imaging to depict the potential DIL which reflects the situation before focal therapy. Interestingly, in the case of multifocal disease, both modalities depicted the same DIL in all patients, which was always the largest lesion in histology. Pucar et al. proved that local recurrence after radiation therapy occurred at the site where MRI showed the primary tumour [1]. Currently no analogous data are available for PSMA PET/CT. Especially in patients with multifocal PCa, multimodal imaging would improve the diagnostic certainty and make it possible to deliver a treatment escalation to the DIL. Additionally, future studies should establish whether multimodal imaging-guided biopsies enhance the detection rate of significant PCa [30].

Our study is limited by the small number of patients and the use of different MRI scanners (1.5 and 3 Tesla). However, we confirmed the data of Eiber et al. [11] using ex-vivo CT for coregistration, which allowed a higher resolution (318 segments in 53 patients vs 340 segments in 7 patients) for data analysis. A known problem in most imaging-pathology correlation studies is the uncertainty in the accuracy of coregistration. One source of inaccurate coregistration is non-linear shrinkage of the prostate due to histopathological preparation. We accounted for this by using non-rigid registration between in- and ex-vivo CTs. There is no ground truth of registration accuracy since the scans were real patient scans. Thus, validation of the registration accuracy was done by comparing prostate contours found in ex-vivo CT (including GTV-histo) and in-vivo CT. We found a good overlap between prostate contours in terms of DSC (mean 0.85) and MD (mean 1.4 mm). However, CT based registration may be impeded by low soft tissue contrast of CT imaging. The usage of ex-vivo MR imaging instead of ex-vivo CT may increase the preciseness of registration [31]. An additional source of inaccurate coregistration is a possible discrepancy in slice angles

between imaging and pathological specimens. By using ex-vivo CT scans in a localizer and a customized cutting device for the prostatectomy specimen, all tissue slices had the same cutting angle as the ex-vivo CT slices. Bladder and bowel motion cause potential movement of the prostate in-vivo. Therefore, exact co-registration of MRI with PET/CT images is difficult. To minimize geometrical errors we used automatic 3D matching tools. Combined PET/MRI scanners may offer a potential benefit due to simultaneous image acquisition [11]. The mentioned systematic uncertainties in coregistration could serve as an explanation for the discrepancy between the good sensitivities/specificities for GTV-MRI and GTV-PET in the segment based analysis and the moderate spatial overlap with GTV-histo, which resulted in low DSC values. Park et al. reported registration errors between 2.26-3.74 mm using ex-vivo MRI for MRI/histology registration [31]. A registration error between 2-4 mm would influence the spatial overlap between the GTVs but not necessarily the sensitivity/specificity in the segment base analysis. In order to account for errors in image coregistration, a previous study applied a 5 mm 3D isotropic margin around each GTV [24]. In analogy to that study we applied a 2.5 mm isotropic margin around each GTV. This led to a slight increase in overlap between enlarged GTV-histo and enlarged GTV-PET (53%), GTV-MRI (46%) and GTV-union (65%), respectively. In a recent study we processed histopathological data on PET resolution to evaluate PET with histology in the same reference frame [5]. Non-processed histopathology models were used in the current study to analyse the coverage of raw PCA lesions and for better comparability with MR images.

Conclusion

Our study performed a slice by slice evaluation between ^{68}Ga -HBED-CC-PSMA PET/CT, mpMRI, and histopathology. For PSMA PET/CT and mpMRI we demonstrated a high sensitivity and specificity for PCa detection. The addition of mpMRI and PSMA PET/CT (GTV-union) increased the sensitivity. The specificity increased if the intersection volume between mpMRI and PSMA PET/CT was considered. For GTV-delineation, the addition of MRI and PET to GTV-union had a significant higher overlap with PCa in histology than both imaging modalities alone. These preliminary findings could have a significant impact on focal therapy approaches as well as for guided biopsy in primary PCa.

Acknowledgements

We would like to thank N. Nanko and his team for the construction of the localizer and the cutting

advice. We would like to thank C. Nolden for his skillful support for spelling and grammar.

Ethical approval

All procedures performed in studies involving human participants were in accordance with the ethical standards of the institutional and/or national research committee and with the 1964 Helsinki declaration and its later amendments or comparable ethical standards.

Informed consent to participate

Informed consent was obtained from all individual participants included in the study.

Informed consent to publish

Informed consent was obtained from all individual participants included in the study.

Competing interests

Author PTM received research grants from Piramal and GE. Author MM received research grants from Philips Medical Systems. Author CZ declares that he has no conflict of interest. Author ALG declares that she has no conflict of interest. Author UW declares that he has no conflict of interest. Author TIB declares that she has no conflict of interest. Author HCR declares that he has no conflict of interest. Author VD declares that she has no conflict of interest. Author MW declares that he has no conflict of interest. Author CAJ declares that she has no conflict of interest. Author WSS declares that he has no conflict of interest. Author MW declares that he has no conflict of interest. Author FS declares that he has no conflict of interest. Author ML declares that he has no conflict of interest. Author MB declares that he has no conflict of interest. Author TK declares that he has no conflict of interest.

References

1. Pucar D, Hricak H, Shukla-Dave A, Kuroiwa K, Drobnjak M, Eastham J, et al. Clinically significant prostate cancer local recurrence after radiation therapy occurs at the site of primary tumor: magnetic resonance imaging and step-section pathology evidence. *Int J Radiat Oncol Biol Phys.* 2007; 69: 62-9.
2. Bott SR, Ahmed HU, Hindley RG, Abdul-Rahman A, Freeman A, Emberton M. The index lesion and focal therapy: an analysis of the pathological characteristics of prostate cancer. *BJU Int.* 2010; 106: 1607-11.
3. Valerio M, Ahmed HU, Emberton M, Lawrentschuk N, Lazzeri M, Montironi R, et al. The role of focal therapy in the management of localised prostate cancer: a systematic review. *Eur Urol.* 2014; 66: 732-51.
4. Bauman G, Haider M, Van der Heide UA, Menard C. Boosting imaging defined dominant prostatic tumors: a systematic review. *Radiother Oncol.* 2013; 107: 274-81.
5. Zamboglou C, Schiller F, Fechter T, Wieser G, Jilg CA, Chirindel A, et al. $(^{68}\text{Ga})\text{HBED-CC-PSMA}$ PET/CT Versus Histopathology in Primary Localized Prostate Cancer: A Voxel-Wise Comparison. *Theranostics.* 2016; 6: 1619-28.
6. Rowe SP, Gage KL, Faraj SF, Macura KJ, Cornish TC, Gonzalez-Roibon N, et al. ^{18}F -DCFBC PET/CT for PSMA-Based Detection and Characterization of Primary Prostate Cancer. *J Nucl Med.* 2015; 56: 1003-10.
7. Rahbar K, Weckesser M, Huss S, Semjonow A, Breyholz HJ, Schrader AJ, et al. Correlation of intraprostatic tumor extent with ^{68}Ga -PSMA distribution in patients with prostate cancer. *J Nucl Med.* 2016; 57: 563-7.

8. Sokoloff RL, Norton KC, Gasior CL, Marker KM, Grauer LS. A dual-monoclonal sandwich assay for prostate-specific membrane antigen: levels in tissues, seminal fluid and urine. *Prostate*. 2000; 43: 150-7.
9. Maurer T, Eiber M, Schwaiger M, Gschwend JE. Current use of PSMA-PET in prostate cancer management. *Nat Rev Urol*. 2016; 13: 226-35.
10. Eder M, Neels O, Muller M, Bauder-Wust U, Remde Y, Schafer M, et al. Novel Preclinical and Radiopharmaceutical Aspects of [68Ga]Ga-PSMA-HBED-CC: A New PET Tracer for Imaging of Prostate Cancer. *Pharmaceuticals (Basel)*. 2014; 7: 779-96.
11. Eiber M, Weirich G, Holzapfel K, Souvatzoglou M, Haller B, Rauscher I, et al. Simultaneous 68Ga-PSMA HBED-CC PET/MRI Improves the Localization of Primary Prostate Cancer. *Eur Urol*. 2016. [Epub ahead of print].
12. Grosu AL, Weirich G, Wendl C, Prokic V, Kirste S, Geinitz H, et al. 11C-Choline PET/pathology image coregistration in primary localized prostate cancer. *Eur J Nucl Med Mol Imaging*. 2014; 41: 2242-8.
13. D'Amico AV, Desjardin A, Chung A, Chen MH. Assessment of outcome prediction models for localized prostate cancer in patients managed with external beam radiation therapy. *Semin Urol Oncol*. 1998; 16: 153-9.
14. Nyul LG, Udupa JK. On standardizing the MR image intensity scale. *Magn Reson Med*. 1999; 42: 1072-81.
15. Weinreb JC, Barentsz JO, Choyke PL, Cornud F, Haider MA, Macura KJ, et al. PI-RADS Prostate Imaging - Reporting and Data System: 2015, Version 2. *Eur Urol*. 2016; 69: 16-40.
16. Woodfield CA, Tung GA, Grand DJ, Pezzullo JA, Machan JT, Renzulli JF, 2nd. Diffusion-weighted MRI of peripheral zone prostate cancer: comparison of tumor apparent diffusion coefficient with Gleason score and percentage of tumor on core biopsy. *AJR Am J Roentgenol*. 2010; 194: W316-22.
17. Mhawech-Fauceglia P, Zhang S, Terracciano L, Sauter G, Chadhuri A, Herrmann FR, et al. Prostate-specific membrane antigen (PSMA) protein expression in normal and neoplastic tissues and its sensitivity and specificity in prostate adenocarcinoma: an immunohistochemical study using multiple tumour tissue microarray technique. *Histopathology*. 2007; 50: 472-83.
18. Wright GL, Jr., Grob BM, Haley C, Grossman K, Newhall K, Petrylak D, et al. Upregulation of prostate-specific membrane antigen after androgen-deprivation therapy. *Urology*. 1996; 48: 326-34.
19. Hamoen EH, de Rooij M, Witjes JA, Barentsz JO, Rovers MM. Use of the Prostate Imaging Reporting and Data System (PI-RADS) for Prostate Cancer Detection with Multiparametric Magnetic Resonance Imaging: A Diagnostic Meta-analysis. *Eur Urol*. 2015; 67: 1112-21.
20. Heidenreich A, Bastian PJ, Bellmunt J, Bolla M, Joniau S, van der Kwast T, et al. EAU guidelines on prostate cancer. part 1: screening, diagnosis, and local treatment with curative intent-update 2013. *Eur Urol*. 2014; 65: 124-37.
21. Zamboglou C, Wieser G, Hennies S, Rempel I, Kirste S, Soschynski M, et al. MRI versus (68)Ga-PSMA PET/CT for gross tumour volume delineation in radiation treatment planning of primary prostate cancer. *Eur J Nucl Med Mol Imaging*. 2016; 43: 889-97.
22. Rhee H, Thomas P, Shepherd B, Greenslade S, Vela I, Russell PJ, et al. Prostate Specific Membrane Antigen Positron Emission Tomography May Improve the Diagnostic Accuracy of Multiparametric Magnetic Resonance Imaging in Localized Prostate Cancer as Confirmed by Whole Mount Histopathology. *J Urol*. 2016. [Epub ahead of print].
23. Thorwarth D, Notohamiprodjo M, Zips D, Muller AC. Personalized precision radiotherapy by integration of multi-parametric functional and biological imaging in prostate cancer: A feasibility study. *Z Med Phys*. 2016. [Epub ahead of print].
24. Chang JH, Lim Joon D, Davis ID, Lee ST, Hiew CY, Esler S, et al. Comparison of [(11)C]choline Positron Emission Tomography With T2- and Diffusion-Weighted Magnetic Resonance Imaging for Delineating Malignant Intraprostatic Lesions. *Int J Radiat Oncol Biol Phys*. 2015; 92: 438-45.
25. Collins AT, Berry PA, Hyde C, Stower MJ, Maitland NJ. Prospective identification of tumorigenic prostate cancer stem cells. *Cancer Res*. 2005; 65: 10946-51.
26. Milosevic M, Warde P, Menard C, Chung P, Toi A, Ishkanian A, et al. Tumor hypoxia predicts biochemical failure following radiotherapy for clinically localized prostate cancer. *Clin Cancer Res*. 2012; 18: 2108-14.
27. Stamey TA, McNeal JE, Freiha FS, Redwine E. Morphometric and clinical studies on 68 consecutive radical prostatectomies. *J Urol*. 1988; 139: 1235-41.
28. McNeal JE, Villers AA, Redwine EA, Freiha FS, Stamey TA. Histologic differentiation, cancer volume, and pelvic lymph node metastasis in adenocarcinoma of the prostate. *Cancer*. 1990; 66: 1225-33.
29. Haffner MC, Mosbrugger T, Esopi DM, Fedor H, Heaphy CM, Walker DA, et al. Tracking the clonal origin of lethal prostate cancer. *J Clin Invest*. 2013; 123: 4918-22.
30. Anastasiadis AG, Lichy MP, Nagele U, Kuczyk MA, Merseburger AS, Hennenlotter J, et al. MRI-guided biopsy of the prostate increases diagnostic performance in men with elevated or increasing PSA levels after previous negative TRUS biopsies. *Eur Urol*. 2006; 50: 738-49.
31. Park H, Piert MR, Khan A, Shah R, Hussain H, Siddiqui J, et al. Registration methodology for histological sections and in vivo imaging of human prostate. *Acad Radiol*. 2008; 15: 1027-39.